PAPER

# Simultaneous Evaluation of Microscopic Defects and Macroscopic 3-D Shape of Planer Object Derived from Specular Reflection Image Sequence

Hidetoshi MIIKE†, *Regular Member*, Sosuke TSUKAMOTO†, *Student Member*, Keishi NISHIHARA†*, *and* Takashi KURODA†**, *Nonmembers*

**SUMMARY** This paper proposes a precise method of realizing simultaneous measurement of microscopic defects and the macroscopic three-dimensional shapes of planar objects having specular reflection surfaces. The direction vector field of surface tilt is evaluated directly by the introduction of a moving slit-light technique based on computer graphic animation. A reflected image created by the moving slit-light is captured by a video camera, and the image sequence of the slit-light deformation is analyzed. The obtained direction vector field of the surface tilt recovers the surface shape by means of integration. Two sample objects, a concave mirror and a plane plastic injection molding, are tested to measure the performance of the proposed method. Surface anomalies such as surface dent and warpage are detected quantitatively at a high resolution (about 0.2 [$\mu$m]) and a high accuracy (about 95%) in a wide area (about 15 [cm]) of the test object.

***key words:*** *specular reflection, active vision, surface defects, 3-D shape*

## 1. Introduction

Recovering three-dimensional (3-D) shapes from visual information is one of the most important issues in the field of computational vision. This problem is divided into two areas of study. One of these areas of study is called passive vision. Only passive information regarding image data from a camera is utilized to extract a 3-D shape. By use of the analogy of the human visual system, several techniques have been established, including shape derived from shading, shape from texture, binocular vision, and motion stereo [1]–[4]. The final goal of these techniques is the understanding of human vision system based on psychology, physiology, and information sciences. The other area of study is active vision or robotic vision [5]–[9]. Recently, increasing attention has been focused on ways to create a realistic virtual image by means of computer graphics. A variety of application fields accelerate the development of this technology; however, a bottleneck exists regarding modeling and measuring the 3-D shape of the real object. A precise and accurate data set describing the 3-D shape is required to reconstruct a realistic virtual world. Especially in cases when we try to represent real objects such as architecture, landscapes, human faces, and plastic injection moldings, we have to introduce an accurate and reliable method for the measurement of the 3-D shape. For this purpose, optical methods such as pattern light sources [5], Moiré-topography [6], and phase shift techniques [7] have been developed. Except for the reflection method of interference optics, most of these methods have been developed for the recovery of a 3-D shape having a diffusive surface. These methods introduce slit-light projection [5], depth from defocus [8], and depth from focus [10]. The maximum resolution of these methods is limited to around 20–100 [$\mu$m]. This level of resolution is satisfactory for the usual purposes of measuring macroscopic 3-D shapes; however, the required resolution to measure the microscopic defects is about 0.1 [$\mu$m], which is difficult to realize using the ordinary direct projection method. On the other hand, several approaches that recover the 3-D shape of an object having a specular surface have been developed (e.g. [11], [12]). However, there are no methods that measure microscopic defects and macroscopic shape simultaneously.

We have been developed a method for recovering the 3-D shape of a planar object having a specular reflection surface [13], [14]. In a previous study [13], we introduced a moving slit-light, which was driven mechanically. The shape of the light source was reflected on the test object having a specular surface, and the light was shifted to the longitudinal direction of the object. The reflected image sequence of the moving slit-light source was obtained by continuous image acquisition. The distribution of the surface tilt angle along the direction and associated surface shape were evaluated by means of image processing. In this approach, however, it is difficult to evaluate surface shape along the direction perpendicular to the longitudinal axis. In present study, we propose a precise method for recovering complete information describing the shape's 3-D structure. The pattern-light sources (x-slit and y-slit), which are synthesized by computer graphic animation (CGA), are

Manuscript received November 9, 2000.
Manuscript revised March 30, 2001.

†The authors are with the Faculty of Engineering, Yamaguchi University, Ube-shi, 755–8611 Japan.
*Presently, with Advanced Science and Technology Center for Cooperative Research, Kyushu University, Kasuga-shi, 816–8580 Japan.
**Presently, with Hitachi Information Systems, Ltd., Tokyo, 150–8540 Japan.

introduced and projected first onto a screen [14]. We observe a mirror image of the slit-light patterns (see Fig. 3) reflected on the object surface. Microscopic defects on the surface of the object are visualized as the deformation of the mirror image of the projected pattern on the screen. This method allows measurement of the direction vector field of the surface tilt of the object. By the integration of the surface tilt, we can evaluate the surface shape. Thus, we realize a simultaneous measurement of microscopic (several [$\mu$m]) defects and macroscopic (several 10 [cm]) shapes of planar objects having specular reflection surfaces. The performance of the proposed method is tested by use of a concave mirror (commercially given) and plastic injection moldings to measure surface anomalies. Surface deformations such as surface dents (several $\mu$m) and warpages (several 100 [$\mu$m]) are detected quantitatively using the proposed method.

## 2. Principle of the Proposed Method

Figure 1 and Fig. 2 show a schematic configuration of the proposed system. The experimental setup is composed of two personal computers (PC), a liquid crystal projector, a screen, a CCD video camera, and a test object. Figure 3 shows two pattern-light sources (x-slit and y-slit) of the moving slit-light synthesized by CGA, and these are projected onto the screen sequentially. The video camera captures a mirror image of the projected patterns on the screen. The pattern-lights on the screen are reflected on the surface of the object. Surface anomalies of the object are visualized as the deformation of the reflected pattern. It should be noted that the pattern deformation is not connected directly to the 3-D shape of the surface. The degree of the deformation directly represents the tilt of the surface. The full surface shape is recovered by the integration of the surface tilt.

First, we consider an object having a flat surface and pick up a point $O$ on the screen (see Fig. 1). Point $O$ is a representative of the projected pattern. Through the object surface (point $P$) the image of the point $O$ is reflected specularly and pictured by the CCD camera. The reflected image of point $O$ is then located at the center of the picture in this configuration. Second, we consider a tilted surface having tilt angle $\beta_y$ [deg] along y-axis as shown in Fig. 1. The reflection point on the object moves from point $P$ to point $S$. This brings a displacement $\delta_y$ [pixel] of the reflected image on the CCD camera. In spite of a difference of system configurations between the previous [13] and the proposed method, we can use the same principle to evaluate the surface anomalies.

On the triangles $\triangle RSP$ and the $\triangle OSP$, we obtain the following relationships:

$$\frac{\sin\gamma}{\overline{PS}} = \frac{\sin\alpha'}{D}, \tag{1}$$

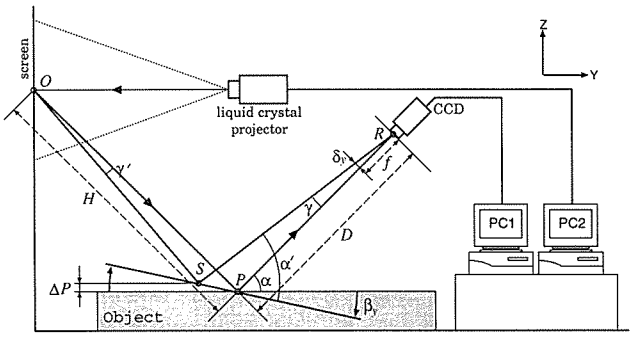


**Fig. 1** A schematic diagram of system configuration with tilt angle $\beta_y$.

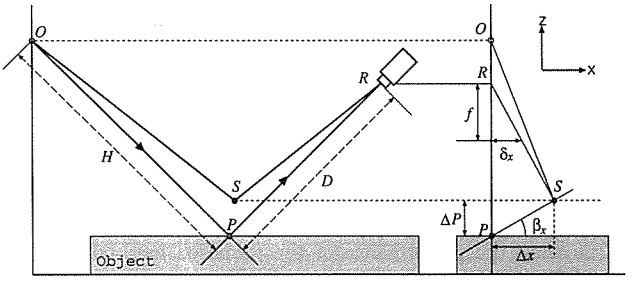


**Fig. 2** A schematic diagram of system configuration with tilt angle $\beta_x$.

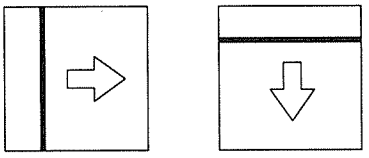


**Fig. 3** Two projected patterns of the moving slit-light source synthesized by computer graphic animation (CGA) on the screen. (a) x-slit and (b) y-slit.

$$\frac{\sin\gamma'}{\overline{PS}} = \frac{\sin(\pi-\alpha')}{H} = \frac{\sin\alpha'}{H}, \tag{2}$$

where $H$ and $D$ represent the distance between the object and the screen and that between the object and the CCD camera, respectively. $\gamma$ and $\gamma'$ are defined as follows:

$$\begin{aligned}\gamma &= \angle SRP = \pi - (\angle SPR + \angle RSP)\\ &= \pi - ((\pi - \alpha - \beta_y) + \alpha')\\ &= \alpha - \alpha' + \beta_y, \end{aligned} \tag{3}$$

$$\begin{aligned}\gamma' &= \angle SOP = \pi - (\angle SPO + \angle OSP)\\ &= \pi - ((\alpha - \beta_y) + (\pi - \alpha'))\\ &= \alpha' - \alpha + \beta_y. \end{aligned} \tag{4}$$

By combining Eqs. (1) and (2), we obtain

$$\overline{PS} = \frac{H\sin\gamma'}{\sin\alpha'} = \frac{D\sin\gamma}{\sin\alpha'}, \tag{5}$$

$$\therefore \quad H\sin(\alpha' - \alpha + \beta_y) = D\sin(\alpha - \alpha' + \beta_y), \quad (6)$$

$$\therefore \quad \frac{\sin(\alpha - \alpha')}{\cos(\alpha - \alpha')} = \frac{\sin\beta_y}{\cos\beta_y} \cdot \frac{H - D}{H + D}, \quad (7)$$

$$\therefore \quad \alpha - \alpha' = \tan^{-1}\left(\frac{H - D}{H + D} \cdot \tan\beta_y\right). \quad (8)$$

When we choose $H = D$, we obtain

$$\begin{aligned}\delta_y &= f \cdot \tan(\gamma) = f \cdot \tan(\alpha - \alpha' + \beta_y) \\ &= f \cdot \tan\beta_y \approx f \cdot \beta_y, \end{aligned} \quad (9)$$

where $f$ is a focal length of the camera. Equation (9) shows a relationship between the tilt angle $\beta_y$ [deg] and the displacement $\delta_y$ [pixel] in two reflected images [13].

Thus, we have an approximate linear relationship between the surface tilt angle $\beta_y$ and the displacement $\delta_y$ for a small angle of $\beta_y$. Consequently, through the measurement of the displacement $\delta_y$, we can determine directly a local surface tilt $\beta_y(x, y)$ on the object. In this configuration (as shown in Fig. 1), we introduce two fundamental assumptions as follows:

1) The size $L$ of the test object, such as the length along longitudinal direction, is known apriori.

2) Amount of surface deformations or anomalies ($\Delta P$) is small compared to the object size ($L$), a distance between the camera and object ($D$) and that between the screen and object ($H$): ($\Delta P \ll L < D \approx H$).

Thus, we can almost fix point $P$ on the surface of the object (see Fig. 1). The failure of this assumption brings an estimation error regarding the surface tilt and associated resolution of surface deformation (see Appendix).

Next, we consider a surface having tilt angle $\beta_x$ along x-axis (see Fig. 2). In the same manner, we can determine a distribution of the local tilt angle $\beta_x(x, y)$ through the measurement of the displacement $\delta_x$. In our previous study [13], we estimated the distribution of surface tilt $\beta_x(x, y)$ and associated surface shape based only on the information of $\delta_y$. In the present study, we use both information regarding $\delta_x$ and $\delta_y$ for a more precise evaluation of the 3-D shape.

Figure 4 shows a simple method for estimating the surface undulation $d(x, y)$ from two data regarding the tilt angles $\beta_x(x, y)$ and $\beta_y(x, y)$. Namely, the following relationships can be reduced under the assumption that the local surface tilt has a constant value:

$$d_x(x + 1, y) = d(x, y) + \Delta x \cdot \tan\beta_x(x, y), \quad (10)$$

$$d_y(x, y + 1) = d(x, y) + \Delta y \cdot \tan\beta_y(x, y), \quad (11)$$

$$d(x+1, y+1) = \frac{d_x(x+1, y+1) + d_y(x+1, y+1)}{2}, \quad (12)$$

where $d_x(x+1, y)$ and $d_y(x, y+1)$ indicate candidates of the deformation evaluated derived from the information of $\beta_x(x, y)$ and $\beta_y(x, y)$, respectively. $\Delta x$ and $\Delta y$ are a magnification [mm/pixel] of the image. We assume that the magnification levels are known prior.

As a reference point, we selected $d_x(x_0, y_0) = 0$. We then estimate the surface undulation $d_x(x_0 + 1, y_0)$ by the integration of the function $\beta_x(x_0, y_0)$ along a x-axis (see Eq. (10) and the arrow of solid line in Fig. 4), and $d_y(x_0, y_0 + 1)$ by the integration of the function $\beta_y(x_0, y_0)$ along y-axis (see Eq. (11) and the arrow of dotted line in Fig. 4). Thus, we have two candidates for the surface undulation $d_x(x_0 + 1, y_0 + 1)$ and $d_y(x_0+1, y_0+1)$. Finally, we estimate the surface shape $d(x_0 + 1, y_0 + 1)$ as the average of these two candidates (see Eq. (12)). We can evaluate the distribution of the surface shape $d(x, y)$ at every point on the object by the repetition of these steps.

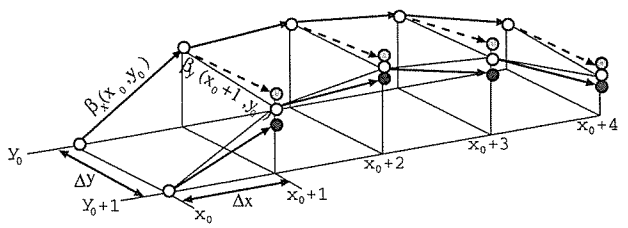


**Fig. 4** Estimation of the surface undulation $d(x, y)$ from two local tilt angles $\beta_x$ and $\beta_y$.

## 3. Experimental System

A block diagram of the experimental system is shown in Fig. 1. Pattern lights are projected on the screen by a liquid crystal projector (SHARP XV-P3Z). Artificial patterns such as slit-light patterns (x-slit and y-slit: see Fig. 3) are created by a personal computer (PC1: NEC PC-9821Ap). Then, a CCD camera (SONY SSC-M370) captures the patterns reflected specularly on the object surface, and PC2 analyzes the 3-D shape with the help of a video acquisition board (Micro-Technica MT98-MN).

We picked up two test pieces. One is a concave mirror. The diameter of the round mirror is 60 [mm$\phi$] and the depth of the depression at the center is 562 [$\mu$m]. The maximum angle of the surface tilt is 2 [deg]. A picture of the mirror is shown in Fig. 5 (a). The other object is an ABS-plastic (TJ3G450) test piece having typical defects of several surface dents and warpage. The plastic was black in color and its surface had a strong luster (specular reflection is superior to diffusive reflection). Figure 5 (b) shows a photograph of the slit-light which is reflected on the surface of the plastic (size is about 150×60 [mm$^2$]).

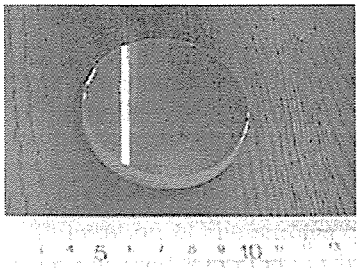

(a) A concave mirror having 562 [$\mu$m] depth at the center.

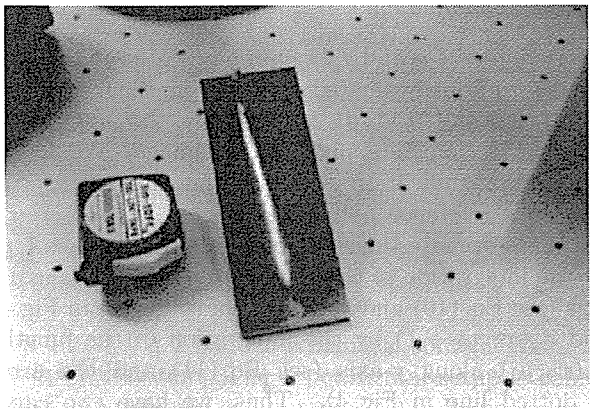

(b) A reflected slit-light reflected on the surface of the plastic test piece.

**Fig. 5** Picture of test pieces.

## 4. Results and Discussion

### 4.1 Calibration Measurement

As a calibration experiment we first used the slit projection pattern to measure a mirror having an optically flat surface (see Fig. 3). All pieces of equipment including the liquid crystal projector, the mirror and the video camera are fixed at a right angle. By tilting the mirror at a given angle $\beta$ [deg], the reflected image of the slit-light shifts $\delta$ [pixel] on the image plane from its primary projection ($\delta$=0). The results of experiment are shown in Fig. 6. The relationship between $\beta$ and $\delta$ is represented approximately by

$$\beta_x/\delta_x \approx 0.043\,[\text{deg/pixel}], \tag{13}$$

and

$$\beta_y/\delta_y \approx 0.032\,[\text{deg/pixel}]. \tag{14}$$

The linear relationship between $\delta$ and $\beta$ is consistent with the theoretical expectation of Eq. (9). The results guarantee the linearity within $\pm 3$ [deg] of surface tilt angle ($\beta$) in our experimental setup. Since the resolutions of image are $\Delta x \approx 0.22$ [mm/pixel] and $\Delta y \approx 0.28$ [mm/pixel], the resolutions of surface undulations $d_x$ and $d_y$ are estimated to be

$$d_x(x, y) = \Delta x \cdot \tan(\beta_x/\delta_x) \approx 0.17\,[\mu\text{m}], \tag{15}$$

and

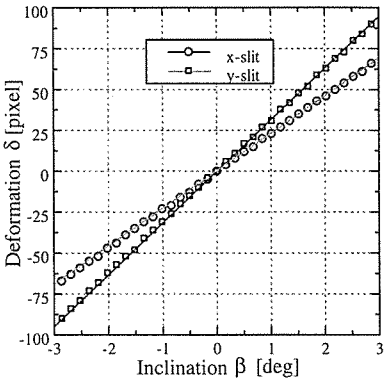


**Fig. 6** A relationship between tilt angle $\beta$ and displacement $\delta$.

$$d_y(x, y) = \Delta y \cdot \tan(\beta_y/\delta_y) \approx 0.16\,[\mu\text{m}]. \tag{16}$$

In this evaluation we neglected the influence of a finite amount of surface deformation $\delta P$. The influence of the deformation ($\delta P \neq 0$) is discussed in Appendix. It is possible to set up to have an appropriate resolution in the measurement by adjusting the camera height, projector height, and the focal length of the camera (see Eq. (9)). In this study we choose $H$=$D$=500 [mm].

### 4.2 Measuring 3-D Shape of a Concave Mirror

Next, we measured the concave mirror in order to determine the accuracy of the proposed method. Figure 7 shows the result of the tilt angle $\beta_x$ and associated undulation $d_x$ along x-axis of the center of the image. Figure 8 shows the result of the tilt angle $\beta_y$ and associated undulation $d_y$ along $y$-axis of the center of the image. The dotted line represents data commercially given (the maximum depth of the concave is 562 [$\mu$m]), and the solid line represents the result of this measurement. The discrepancy of the results is small between those measured and those commercially given. The surface shape of the concave mirror is well recovered, as shown in Fig. 9. The 3-D shape of the mirror is visualized from the given data (Fig. 9 (a)) and from the measured data (Fig. 9 (b)). Thus, the accuracy of the proposed method is confirmed by the measurement of the concave mirror with a known shape. The maximum discrepancy of the absolute undulation between the measured data and the given data is about 30 [$\mu$m]. Thus, the accuracy of the measurement is about 95% ($= (-30/562) \times 100\%$). This discrepancy may be due to the accumulation error of undulation evaluation (see Eqs. (10)–(12)) and the deviation of the dimensions of the optically polished mirror from the given specifications.

### 4.3 Measuring 3-D Shape of a Plastic Moldings

A sequence of the observed reflected images of the x-slit light source and y-slit source on a plastic test piece

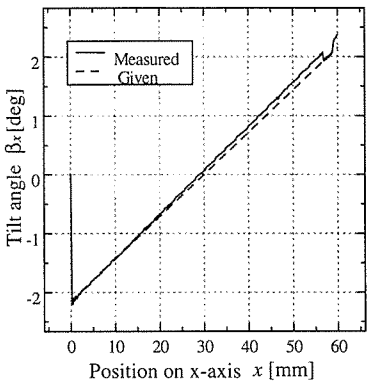


(a) Distribution of tilt angle $\beta_x$.

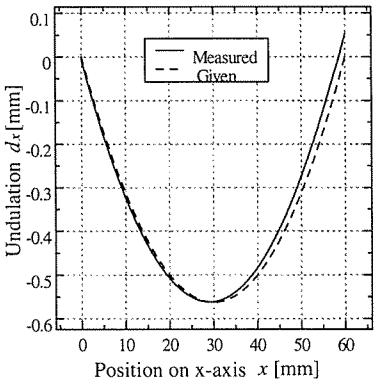


(b) Distribution of undulation $d_x$.

**Fig. 7** The measured and given tilt angle $\beta_x$ and associated undulations $d_x$ along x-axis.

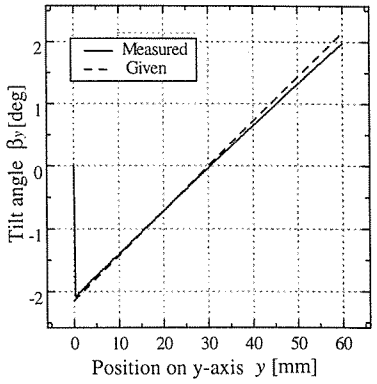


(a) Distribution of tilt angle $\beta_y$.

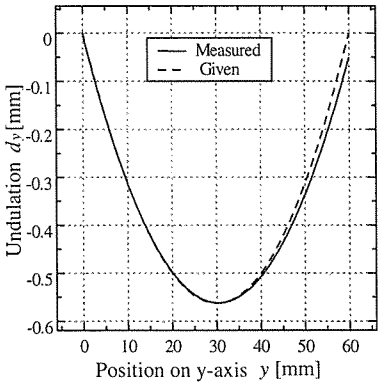


(b) Distribution of undulation $d_y$.

**Fig. 8** The measured and given tilt angle $\beta_y$ and associated undulations $d_y$ along y-axis.

((a)–(h)), and its schematic explanation (i) are shown in Fig. 10. These images have 256 levels of gray value and are 508×190 [pixels] in size. We captured the x-slit image sequence of 210 [frame] and the y-slit image sequence of 120 [frame] using a sampling frequency of 1 [Hz]. The x-slit light moves from left to right and the y-slit light moves from top to bottom with a constant velocity on the screen (see Figs. 10 (a)–(h)).

The plastic is placed on a flat mirror (see Fig. 10 (i)). The reflections from the mirror retrieve information regarding the reference points. An intersection point of x-slit and y-slit on the mirror represents an ideal position $P$, where the surface has no tilt. An intersection point of x-slit and y-slit on the plastic represents a displaced position $S$ (see Fig. 1). We estimate the displacement $\delta_x$ and $\delta_y$ by measuring the distance from the ideal point $P$ to the point $S$, and we can determine the surface tilt angles $\beta_x$ and $\beta_y$ using Eqs. (13) and (14).

In Fig. 10 (b), the existence of a small circular dent is visualized in the middle of the reflected slit image, and (c) and (d) show reflected slit-lights split by the influence of a large dent. Applying the proposed method to the obtained image sequence, we measured surface defects. The results are summarized in Fig. 11. In the distribution of surface tilt $\beta(x, y)$, we can recognize the

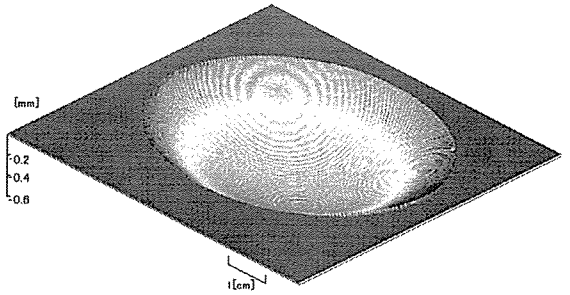


(a) Commercially given data.

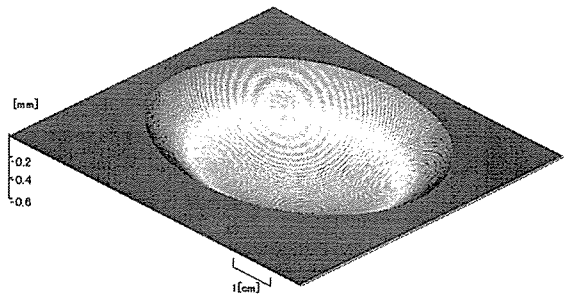


(b) Measured data obtained by the proposed method.

**Fig. 9** Undulation $d(x, y)$ of a concave mirror.

local structure of surface defects such as surface dents (see the arrowed positions in Fig. 11 (a) and 11 (b)). The local shape of the small dent is detected quantita-

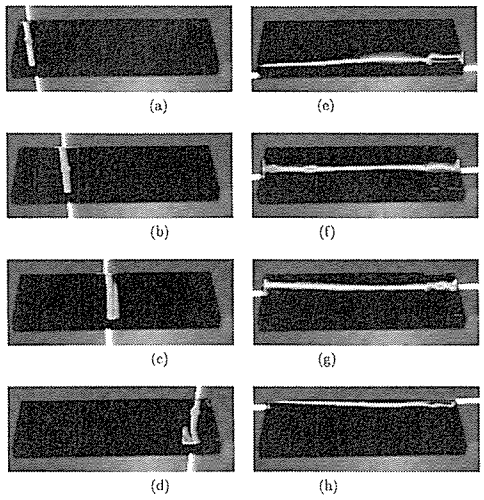


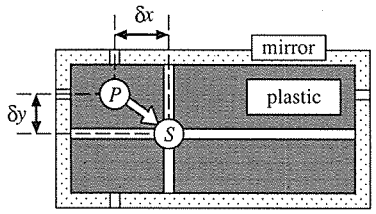


(i) A schematic illustration of the actual measurement.

**Fig. 10** Examples of the reflected images on a plastic test piece. (a)–(d) Reflected images using x-slit. (e)–(h) Reflected images using y-slit.

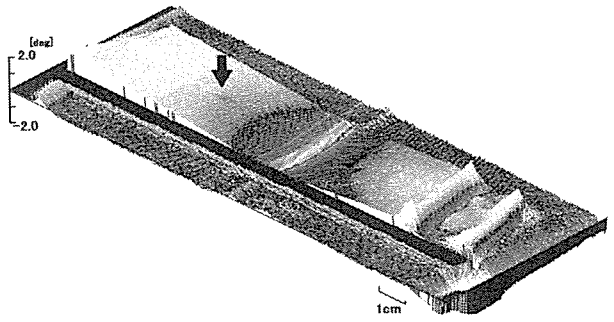


(a) Distribution of tilt angle $\beta_x(x, y)$

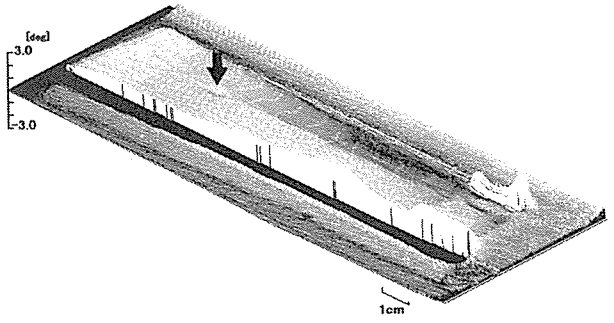


(b) Distribution of tilt angle $\beta_y(x, y)$

**Fig. 11** Results of measurement of tilt angle $\beta$ using slit-light patterns. Arrows show the position of a small surface dent visualized by the proposed method.

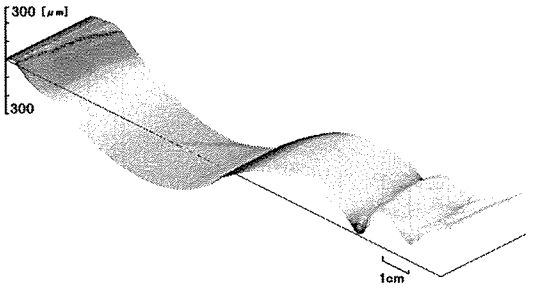


**Fig. 12** Result of undulation measurement $d$ (macroscopic surface shape) estimated by tilt angle distributions $\beta_x$ and $\beta_y$.

tively. The radius and the depth of the dent are determined to be 1.0 [cm] and 1.2 [$\mu$m], respectively. On the other hand, in the distribution of surface undulation of surface shape $d(x, y)$, we recognize the global structure of a surface deformation such as warpage (see Fig. 12). A small deformation along the longitudinal direction is visualized quantitatively. The maximum deformation is more than 300 [$\mu$m]. Thus, we obtain a quantitative picture of the surface shape. Not only a microscopic defect composed of a small surface dent (about 1 [$\mu$m]) but also the global structure of the object's warpage (about 500 [$\mu$m]) is captured simultaneously using the proposed method. In contrast to the size resolution of the image (about 0.3 [mm/pixel]), the minimum resolution of surface roughness (about 0.2 [$\mu$m]: see Appendix) is rather surprising. As discussed in our previous report [13], the reflected image from the specular surface is sensitive to surface anomalies. The proposed method enables us to measure the distribution of the surface tilt vector directly.

## 5. Concluding Remarks

In this paper, we introduce a new system configuration as shown in Fig. 1. The artificial pattern of moving slit-lights is projected onto a screen. The light is not projected directly onto the test object. This is a key point of the proposed method. The camera observes a mirror image of the pattern reflected specularly on the object surface. Defects and/or deformations of the object are visualized as deformations in the mirror image of the projected pattern. Compared to the conventional methods (e.g. the direct projection method of patterned light sources), the proposed system configuration has the following several advantages:

1) Compatibility of shape detection in a wide observation area and resolution of surface roughness through an observation camera.

2) Flexible pattern projection including sequential projection of x-slit and y-slit lights.

The latter advantage provides a precise method for

measuring the 3-D shape of a planar object having a specular reflection surface. By the introduction of CGA technique, the direction vector field of surface tilt $\beta_x(x, y)$ and $\beta_y(x, y)$ is evaluated. The surface shape is recovered by the transformation of the vector field to surface undulation $d(x, y)$. To confirm the performance of the proposed method, we picked up two sample objects, a concave mirror and a plane plastic injection molding. The main points of the results are summarized as follows.

1) Through calibration experiment using a flat mirror, the maximum resolution of surface undulation was estimated to be about 0.2 [$\mu$m].

2) The accuracy of shape measurement was tested by the use of a concave mirror (optically polished) having a 562 [$\mu$m] hollow at the bottom of the mirror. The maximum discrepancy between the measured data and that commercially given is about 30 [$\mu$m]. The accuracy of the measurement was estimated to be about 95%.

3) Surface anomalies on a sample plastic molding are observed quantitatively. Microscopic or the local structure of a surface dent was well visualized in the surface tilt images $\beta_x(x, y)$ and $\beta_y(x, y)$. Macroscopic or global structure of warpage was well captured in the undulation image $d(x, y)$.

Thus we realize simultaneous detection of the macroscopic relative shape and microscopic surface anomalies of a planar object having a specular surface. In spite of the low resolution of the camera image (about 0.3 [mm/pixel]), it is possible to measure microscopic defects (about 0.2 [$\mu$m]) and surface anomalies in a wide area (about 15 [cm]) of the test object.

## Acknowledgements

The authors wish to express their heartfelt thanks to Dr. T. Sakurai and Mr. H. Ikemoto for their experimental help. We are also indebted to Prof. K. Koga, Dr. K. Nakajima, and Dr. E. Yokoyama for their invaluable discussions.

### References

[1] T. Wada, H. Ukida, and T. Matsuyama, "Shape from shading with inter-reflections under proximal light source," Proc. ICCV'95, pp.66–71, 1995.
[2] R. Horaud and T. Skordas, "Structural matching for stereo vision," Proc. ICPR'88, pp.439–445, 1988.
[3] H.Z. Dan and B. Dubuisson, "String matching for stereo vision," Patt. Recognit. Lett., vol.9, pp.117–126, 1989.
[4] R. Navatia, "Depth measurement from motion stereo," Proc. CGIP'76, vol.9, pp.203–241, 1976.
[5] N. Okada and T. Nagata, "A range finder with two cameras and a laser slit marker and its calibration," IEE Trans. Japan, vol.116-C, no.6, pp.684–691, 1996.
[6] H. Takasaki, "Moiré topography," Appl. Opt., vol.9, pp.1467–1471, 1970.
[7] K. Omura, K. Tsukamoto, and S. Nakadate, "Application of real time phase shift interferometer to the measurement of concentration field," J. Crystal Growth, vol.129, pp.706–718, 1993.
[8] P. Grossmann, "Depth from focus," Patt. Recognit. Lett., vol.5, pp.63–69, 1987.
[9] M. Oren and K. Nayar, "A theory of specular surface geometry," Proc. ICCV'95, pp.740–747, 1995.
[10] B. Jähne, Digital Image Processing, 2nd ed., pp.233–237, Springer-Verlag, 1995.
[11] Z. Wang, H. Kato, K. Sato, and S. Inokuchi, "Three dimensional measurement of specular objects," IEICE Trans., vol.J75D-II, no.7, pp.1177–1186, July 1992.
[12] T. Miyake, K. Umemura, and S. Sato, "A technique for reconstructing shape of specular objects," Proc. IAPR Workshop on Machine Vision Applications (MVA 92), pp.599–602, 1992.
[13] H. Miike, K. Koga, T. Yamada, M. Kitou, T. Kawamura, and N. Takikawa, "Measuring surface shape from specular reflection image sequence," Jpn. J. Appl. Phys., vol.34, pp.1625–1628, 1995.
[14] M. Goto, H. Miike, T. Kuroda, T. Kawamura, M. Kitou, and N. Takikawa, "Measuring 3-D shape based on specular image sequence procession with sinusoidal pattern light source," Proc. 2nd Image Sensing Symposium, pp.41–46, 1996.

## Appendix

In this text, we assume that the measurement point $P$ is fixed very closely to the object having a flat plane. When the object has surface anomalies or deformations, however, point $P$ divides the original plane. As depicted in Fig. 1 and Fig. 2, the deformed point $S$ is not on the original (surface) plane. This failure of assumption constitutes a limit of resolution and/or tilt angle error. Next we consider a configuration as shown in Fig. A·1. We can estimate the influence of surface deformation for the estimation error of the surface tilt angle $\beta$. When we have the discrepancy $\delta_x$, we can not distinguish $P$ and $P'$ through the camera. This results in an error of the surface tilt $\delta\beta$. Solving the geometric configuration we obtain the following relationship:

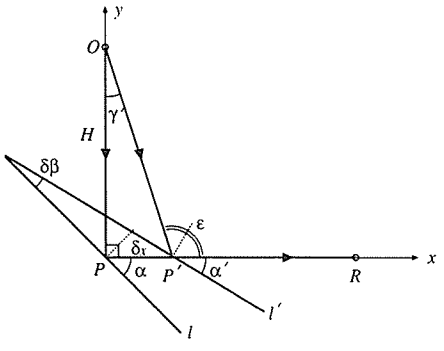


**Fig. A·1** A geometric configuration describing a limit of angular resolution to measure surface tilt.

$$\delta\beta = \alpha - \alpha' = \frac{\gamma'}{2} = \frac{1}{2}\tan^{-1}\left(\frac{\delta x}{H}\right), \qquad (A\cdot 1)$$

where

$$\begin{cases} \alpha &= \pi/4 \\ \alpha' &= \pi/2 - \epsilon/2 \\ \epsilon &= \gamma' + \pi/2 \end{cases} \qquad (A\cdot 2)$$
$$\therefore \quad \delta\beta = \frac{\pi}{4} - \frac{\pi}{2} + \frac{\epsilon}{2} = \frac{\gamma'}{2}.$$

When we choose $H$=500 [mm], $\delta_x$=1 [mm],

$$\delta\beta = \frac{1}{2}\tan^{-1}\left(\frac{\delta x}{H}\right) \approx 0.0573\,[\text{deg}]. \qquad (A\cdot 3)$$

Following Eq. (15), we can estimate $d(x,y) = \Delta x \cdot \tan(\beta_x/\delta_x) \approx 0.2\,[\mu\text{m}]$. This can be a limit of resolution under the configuration ($H$=$D$=500 [mm], $\delta x \approx$ 1 [mm]). In this study we picked up planar objects having small deformations ($\delta x < 1.0$ [mm]). Thus, the limit of resolution is less than 0.2 [$\mu$m]. If we choose a suitable geometrical configuration we can measure a surface shape having an enhanced deformation.

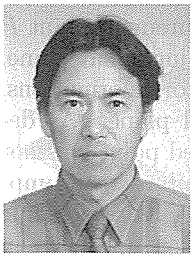

**Hidetoshi Miike** received the B.E. degree in 1971, M.E. degree in 1973, and the Dr. Eng. degree in electronics in 1976, all from the Kyushu University, Fukuoka, Japan. In 1976, he joined Faculty of Engineering, Yamaguchi University. Since 1991, he has been a Professor of the university. His research interests include information sciences, vision engineering, nonlinear sciences and fluid dynamics. He is a member of IPS Japan, Physical Society of Japan, IEEE computer society, and American Association for the Advancement of Science.

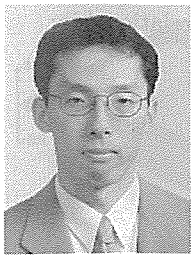

**Sosuke Tsukamoto** is a doctor course student in Yamaguchi University, Japan. His research interests include computer vision and neural networks. He received the B.E. degree in electronics from Hiroshima Institute of Technology, Japan, in 1996 and the M.E. degree in computer sciences and systems engineering from Yamaguchi University, Japan, in 1998.

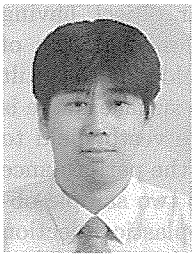

**Keishi Nishihara** received his Dr. in engineering in 1997 from Kyushu University, Fukuoka, Japan. He worked in Yamaguchi University from 1998 to 2000 in the area of vision engineering, nonlinear sciences and fluid dynamics. He became a research associate at Kyushu University in 2000. His research interests include optical measurement, vision engineering, fluid dynamics and heat pump type air conditioning system. He is a member of Japan Society of Applied Physics.

**Takashi Kuroda** received the B.E. and M.E. degrees in electrical and electronic from Yamaguchi University, Japan, in 1996 and 1998, respectively. His research interests include computer vision and signal processing. He is currently working at Hitachi Information Systems, Ltd., Japan.